International Journal of Heat and Mass Transfer 166 (2021) 120746

Contents lists available at ScienceDirect

International Journal of Heat and Mass Transfer

journal homepage: www.elsevier.com/locate/hmt

Bayesian Method for Parameter Estimation in Transient Heat Transfer Problem

Aminul Islam Khan, Md Muhtasim Billah, Chunhua Ying, Jin Liu, Prashanta Dutta*

School of Mechanical and Materials Engineering, Washington State University, Pullman, WA 99164-2920

ARTICLE INFO

Article history:
Received 26 July 2020
Revised 19 November 2020
Accepted 21 November 2020

Keywords:
inverse problem
steam header
Metropolis–Hastings algorithm

ABSTRACT

Like many other scientific fields, an inverse technique is used to find unknown material properties (such as thermal conductivity, specific heat) or boundary conditions (e.g. heat flux, heat transfer coefficient) in the heat transfer problem. The role of the inverse technique is even more important if the properties or boundary conditions change with location and/or time. In this study, a Bayesian inference based inverse technique is used to find local heat transfer coefficient as well as local steam temperature at the inner surface of a steam header where the header was first heated by supplying steam followed by the cooling of the header due to the release of steam from the chamber. A finite volume based numerical model is developed to solve the forward unsteady heat conduction problem in the steam header. For inverse problem, a Markov chain Monte Carlo method is used to evaluate the posterior probability density functions (PPDFs) of unknown parameters in Bayesian framework, while a Metropolis-Hastings algorithm is used for random sample generation. Here PPDFs are used to extract the point estimates of the parameters and their credible intervals from their possible distributions. With the estimated parameters, the calculated outer surface temperatures agree well with experimental measurements in both heating and cooling process. At the end of the discharge process, the temperature distribution in the radial direction approaches flat profiles, but a steady state is only achieved at the bottom of the header. *Our stochastic based Bayesian technique can be used to estimate unknown boundary conditions efficiently at an inaccessible location.*

1. Introduction

While the idea of an inverse technique was proposed more than a century ago, it has gained much more attention over the last few decades due to remarkable advancement in computational capability. An inverse technique is very useful for acquiring information in scenarios when a system parameter cannot be readily measured or a location cannot be physically accessed [1]. It can be used to achieve insights about the physical problem in terms of the estimated model parameters from a set of experimentally measured or observable data. Some of the commonly used early inverse techniques includes the least squares method [2], Kalman filtering [3], linear quadratic estimation (LQE), and shooting algorithm [4,5].

In modern times, inverse techniques have seen broad applications in numerous fields. For instance, these techniques are extensively used in oceanography for ocean circulation and acoustics [6-10], in petroleum engineering for reservoir characterization and oil shale modeling [11-13], in satellite meteorology for weather forecast [14], in hydrology for characterizing the hydrodynamic behavior and predicting transport in an aquifer [15,16], in biomedical engineering for computer tomography and imaging [17-20] etc. With the applications spanning over diverse fields, the necessity for new methods that are more powerful in terms of efficacy have been established. For example, in recent years more efficient methodologies such as the quasi Newton method [21], the preprocessing method [22], control volume based method [23], artificial neural network [24,25], and deep learning based techniques [26,27] have been developed for inverse problems. *However, these methods neither consider sources of uncertainty in the estimation process nor quantify the uncertainties included in the estimated results.*

Bayesian method [28,29] provides a solution to the problem of quantifying uncertainties in parameter estimation process. In recent years, Bayesian method has been extensively used in bioinformatics for gene expression analysis [30], flood modeling [31], modeling of biophysical systems [32-34], econophysics for stock market prediction [35,36] and many more due to improved computational capabilities and advanced numerical sampling techniques, such as the Markov chain Monte Carlo method [37]. Over the last two decades, Bayesian method has also been applied in the heat transfer regimes for determining boundary conditions that are physically inaccessible or for estimating parameters that are not mea-

* Corresponding author. Tel: (509) 335-7989; Fax: (509) 335-4662
E-mail address: prashanta@wsu.edu (P. Dutta).

https://doi.org/10.1016/j.ijheatmasstransfer.2020.120746
0017-9310/

Nomenclature

ρ	Density of the material, kg/m^3
C_P	Specific heat capacity, J/kgK
t	Time, sec
$r,\ \theta$	Polar coordinates
T	Temperature at position $(r,\ \theta)$ and time t, °C.
k	Thermal conductivity, W/mK
$e_r,\ e_\theta$	Unit vectors in r and θ directions, respectively
$\vec{J}$	Heat flux through a control volume face, W/m^2
r_i	Inner radius of the header wall, m
r_o	Outer radius of the header wall, m
q	Heat flux, W/m^2
h	Convective heat transfer coefficient, W/m^{2}K
T_i	Temperature on header inner surface, °C
T_{st}	Steam temperature, °C
ϕ	Unknown parameter vectors
$\hat{\phi}$	Mean of unknown parameter vector ϕ
a_r	Acceptance ratio
E	Expectation
∇	Divergence
T_E	Set of observed temperatures
T_M	Set of model temperatures
ε	Model error
ν_{ij}	Variance of model error
σ_{ij}	Standard deviation of model error
n	Number of spatial points
m	Number of temporal points
$\Re$	Parameter space
I	Indicator function
ψ	Transition density function
α	Acceptance probability
r_N	Random number $\in (0, 1)$
φ	Unknown physical parameter vector
K	MCMC iteration number
$\mathbb{N}$	Normal distribution function
p	Probability
U	Uniform distribution function

surable [38,39]. For example, Iglesias et al. [40] estimated the thermal resistance and heat capacity under different initial conditions; Raj et al. [41] determined specific heat capacity and emissivity of a solid material; and Wang et al. [42] calculated heat flux through a wall from temperature measurements. *However, none of these previous works were applied for finding time dependent local parameters. In this work, we use the Bayesian inference approach to estimate local heat transfer coefficients and steam temperatures along the inner surface of a steam header based on the experimentally measured temperatures at the outer surface.* The physical problem is adopted from a transient heat conduction experiment carried out by Duda [23] in a steam header (see Fig. 1). In our Bayesian formulation, the posterior distribution of the unknown parameters is approximated by Markov chain Monte Carlo method where the Metropolis-Hastings algorithm [43,44] is used for sampling posterior distribution of these parameters. The whole procedure is executed in R [45] using an in-house numerical model.

The rest of the paper is organized as follow. We first present the mathematical model for both forward and inverse problems as well as the relevant methods used for both problems. Next, we verify our finite volume method (FVM) developed for the forward problem by comparing our results with the ANSYS predictions presented in Ref. [23] for an identical system. Here, it is important to note that the problem addressed by Bayesian method is completely different from the one solved to verify the FVM formulation. The verified FVM is used in Bayesian inference to estimate unknown local heat transfer coefficients and steam temperatures during transient heat transfer in a header using the experimental measurements given in Ref. [23]. Once the local heat transfer coefficients and steam temperatures are determined, the temperatures at the inner surface are readily obtained from finite volume

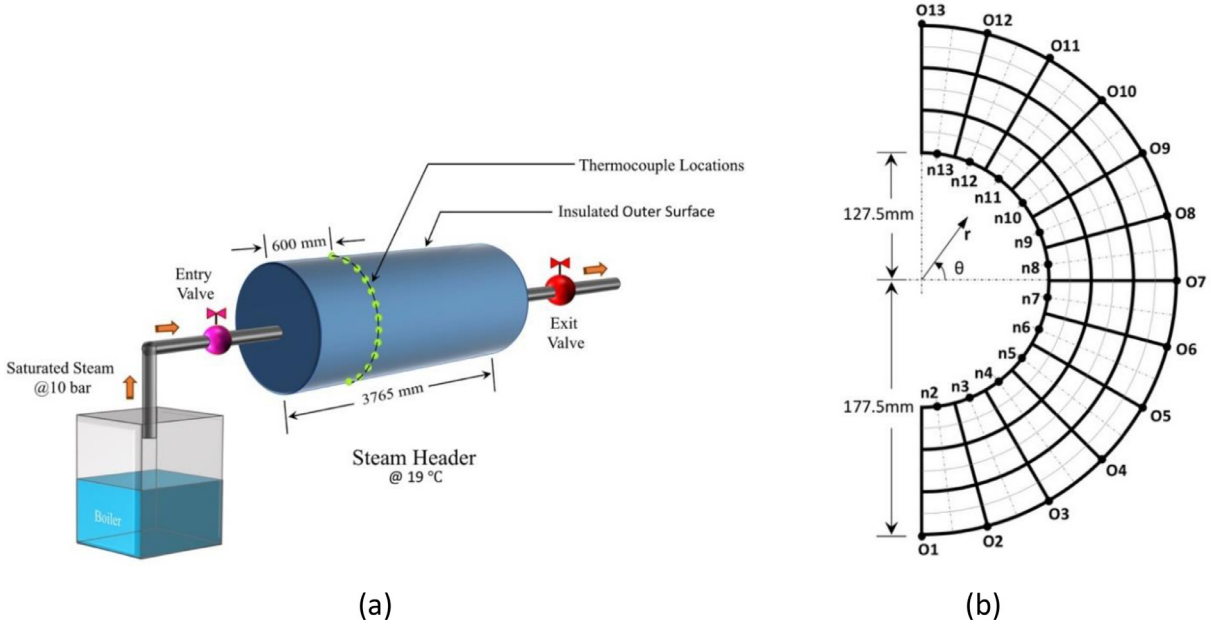

Fig. 1. (a) Schematic of the steam header showing the entry and exit valves and the location of the 13 thermocouples on the insulated outer surface. The header is initially maintained at 19 °C. For $t \leq 580$ sec, the inlet valve remains open and exit valve remains closed which is called the charging of steam header. For $t > 580$ sec, the inlet valve remains closed and exit valve remains open which is called the discharging of the header. (b) Division of steam header into control volumes (CVs) in polar coordinates (r, θ). The entire wall of the header has been divided into finite number of CVs and only 12 inner boundary points ($n2 - n13$) are shown in this figure since these are the points of interest. Temperatures were measured at the outer 13 node points (denoted by $O1 - O13$).

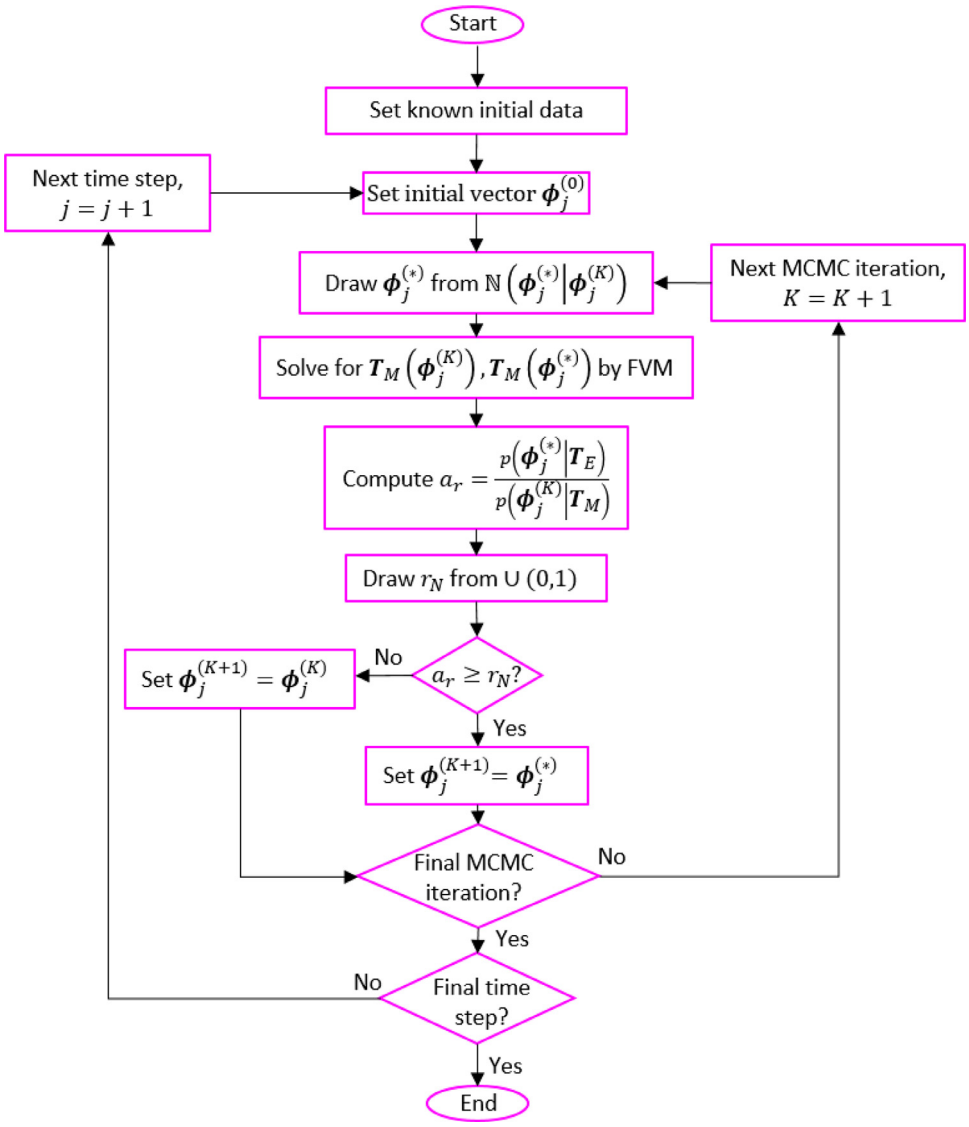

Fig. 2. Flowchart of the Metropolis-Hastings algorithm.

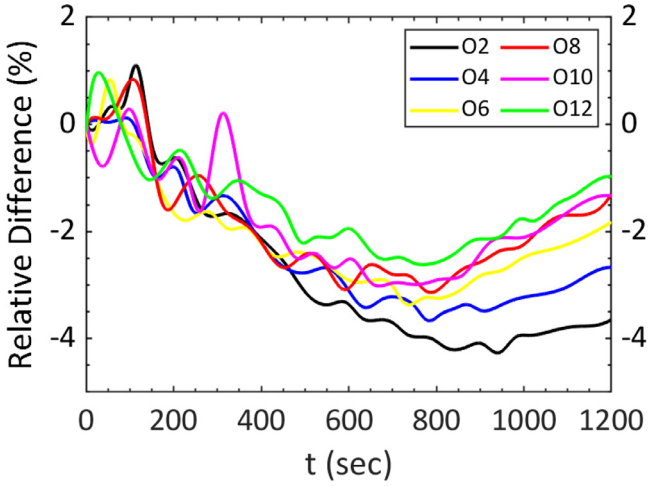

Fig. 3. Percentage of relative difference between two numerical calculations carried out using ANSYS in Ref. [23] and our finite volume method - using the formula $(T^i_{FVM} - T^i_{ANSYS})/T^i_{ANSYS}$ where T^i_{FVM} are the temperatures from our finite volume method, T^i_{ANSYS} are the corresponding temperatures from the simulations in ANSYS and $i = 1, 2, 3, \ldots, 13$. Results are only shown for 6 nodes (for better visibility) on the header (outer) surface.

discretized equations. To achieve a better insight, the temperature profiles along the radial direction of the steam header wall are also provided.

2. Mathematical modeling

2.1. Transient heat conduction through steam header

The physical problem considered in this study is based on a previous work of Duda [23], where a steam header (Fig. 1(a)) was first heated by supplying saturated steam from a boiler at a pressure of 10 bar. The initial temperature of the steam header was 19°C, and steam was supplied to the steam header continuously for 580 sec. Then the exit valve of the steam header was opened, which caused a decrease in pressure inside the header as steam and condensate left the header until it reaches an equilibrium with the atmosphere. Thus, the entire heat transfer phenomena can be divided into two parts: the first part is the charging of steam header (inlet valve open and exit valve closed), while the second part is the discharging of the header (inlet valve closed and exit valve open). In their experiments, the outer surface temperature was measured at 13 points during the heating/cooling process of the steam header. These 13 points, which constitute 12 control volumes (CVs) for modeling purpose, are presented in Fig. 1(b). The

steam header was made of martensitic P91 steel, and the temperature dependent properties such as thermal conductivity, specific heat, etc. are adopted from Ref. [23].

2.2. Governing equations

A cylindrical coordinate system has been used to model the transient heat transfer through the thick wall of the steam header. The minimal heat transfer along the axial direction of the header has been ignored and thus the heat transfer has been assumed to be two dimensional (in r and θ directions only). In the absence of heat source, the temperature distribution through the steam header cross section can be described as:

$$\frac{\partial(\rho C_P T)}{\partial t} = \nabla \cdot (k \nabla T) \tag{1}$$

where ρ, C_P and k denote the density, the specific heat capacity and the thermal conductivity of the material, respectively. For polar coordinates, the operator ∇ can be expressed as,

$$\nabla = \frac{\partial}{\partial r} e_r + \frac{1}{r}\frac{\partial}{\partial \theta} e_\theta \tag{2}$$

where e_r and e_θ are the unit vectors in r and θ directions, respectively. Rearranging equation (1) and (2),

$$\frac{\partial(\rho C_P T)}{\partial t} + \nabla \cdot \vec{J} = 0 \tag{3}$$

where $\vec{J} = -k \nabla T$ is the heat flux through a face of the control volume.

2.3. Boundary conditions

In our model only half of the cross section is considered due to symmetry. The outer surface of the header was thermally insulated during the experiment (after the installation of the thermocouples), which is included in the model. Also, because of symmetry, both at $\theta = -\frac{\pi}{2}$ and $\theta = \frac{\pi}{2}$, insulated boundary condition is considered. Thus, the boundary conditions for the model are,

$$\begin{aligned} &@\ r = r_i,\ q = h(T_{st} - T_i) \qquad @\ r = r_o,\ \tfrac{\partial T}{\partial r} = 0 \\ &@\ \theta = -\tfrac{\pi}{2},\ \tfrac{\partial T}{\partial \theta} = 0 \qquad @\ \theta = \tfrac{\pi}{2},\ \tfrac{\partial T}{\partial \theta} = 0 \end{aligned} \tag{4}$$

where r_i and r_o are the inner and outer radius of the header, respectively. $\theta = -\frac{\pi}{2}$ and $\theta = \frac{\pi}{2}$ denote the bottom and top points on the header surface, respectively, along the circumferential direction. In the beginning, the entire system was maintained at 19 °C and thus the initial condition for the problem is,

$$@t = 0,\ T = 19^\circ C \tag{5}$$

This problem can be solved using FVM method, however, we do not know the parameters h and T_i. Therefore, we use Bayesian inference technique to estimate these parameters.

3. Bayesian framework for the inverse problem

Determination of the posterior probability density functions of parameters is the primary interest of Bayesian inference method. Bayesian inference uses two sources of information: observed data and available prior knowledge to learn about the posterior probability density functions of unknown parameters. The unknown parameters vector φ is considered as a variable, and the available knowledge about those parameters before knowing the observed data is expressed by the prior probability density function $p(\varphi)$. After observing/knowing the data, experimentally measured temperature at the outer surface of the header, T_E, the posterior probability density functions of parameters $p(\varphi|T_E)$ can be described by Bayes theorem as,

$$p(\varphi|T_E) = p(T_E|\varphi)p(\varphi)/p(T_E) \tag{6}$$

where $p(T_E)$ is a proportionality constant so that $\int p(\varphi|T_E)d\varphi = 1$ and $p(T_E|\varphi)$ is the likelihood which measures how well the model fits to the observed data for given values of the unknown parameters.

3.1. Likelihood

There are two types of errors that can be considered in the model. First, the error occurs due to experimental protocols such as intrinsic error of sensors. Second, the error arises due to assumptions used in the model. With these errors, the true value of variables (here it is temperature) can be given as [46]

$$T_E = T_{tr} + \varepsilon_E \tag{7}$$

$$T_M(\varphi) = T_{tr} + \varepsilon_m \tag{8}$$

where T_E, T_{tr} and $T_M(\varphi)$ are experimentally measured temperature, true physical temperature and temperature produced by the model, respectively. ε_E and ε_m are errors associated with experimentally measured temperature and model predicted temperatures, respectively. Since we know very little about the experimental data (as we didn't conduct the experiment), we consider experimentally measured temperature to be equal to the true physical temperature ($T_E = T_{tr}$) i.e. there is no error in experimentally measured temperature ($\varepsilon_E = 0$). Therefore, equations (7) and (8) can be combined as

$$T_E = T_M(\varphi) + \varepsilon \tag{9}$$

where, $\varepsilon_m = \varepsilon$ and $T_E = \{T_{E,ij} : i = 1,\ 2, \ldots, n\ ;\ j = 1,\ 2,\ \ldots,\ m\}$. The error term ε_{ij} is assumed to be a normally distributed random variable with zero mean and variance of $v_{ij} = \sigma_{ij}^2$ where σ_{ij} is the standard deviation of model error. Therefore, under this assumption, the likelihood function $p(T_E|\varphi)$ can be expressed as [33]

$$p(T_E|\varphi) = \prod_{ij} \left(2\pi\sigma_{ij}^2\right)^{-0.5} exp\left\{ -\frac{\left[T_{E,ij} - T_{M,ij}(\varphi)\right]^2}{2\sigma_{ij}^2} \right\} \tag{10}$$

Since we aim to estimate unknown parameters φ for each temporal point, the above equation can be written for (n) spatial points as

$$p(T_E|\varphi) = \left(\prod_{i=1}^{n} \left(2\pi\sigma_i^2\right)^{-0.5} \right) exp\left\{ -\frac{1}{2} \sum_{i=1}^{n} \frac{[T_{E,i} - T_{M,i}(\varphi)]^2}{\sigma_i^2} \right\} \tag{11}$$

3.2. Prior

Usually, inverse problems, such as the present one, are ill-posed and require regularization for a stable solution. Therefore, instead of solving an ill-posed problem, a regularized approximate well-posed problem is solved in this study. In Bayesian frameworks, the regularization for the ill-posed inverse problem can be done in the prior information. To choose the prior, we have followed the plausible bounds method described by Choi et al. [46]. The minimum and maximum limit of priors (i.e. the range of a parameter) was carefully set with physical/known information. For example, we have prior knowledge that saturated steam at a pressure of 10 bar is entering into the header at the beginning of the charging process. Therefore, for the charging process, the plausible range for unknown steam temperature at any time (t) is set between temperature of steam at previous time ($t - \Delta t$) and 30°C above the saturation temperature corresponding to header pressure at time t. For discharging process, the pressure inside the header is around atmospheric pressure, therefore the plausible range is set between temperature at the start of discharge process and 30°C below the saturation temperature corresponding to atmospheric pressure. For

the unknown heat transfer coefficient, we set a range between zero and $20,000 \mathrm{W/m^2{}^\circ C}$ as estimated in Ref. [23]. Furthermore, as condensed water is accumulated in the lower part of the header due to gravity, nodes at the lower part of header are initialized with smaller heat transfer coefficient, while nodes at the upper part of header are initialized with larger heat transfer coefficient. The standard deviation of model error, σ_i is also treated like other unknown parameters by defining a new parameter vector $\phi = \{\varphi, \sigma\}$. The upper bound of standard deviation of model error is considered to be an arbitrary large value (such as 10) while the lower bound is set as zero. With this carefully chosen plausible range, an informative prior distribution can make the inverse problem robust. However, even with carefully constructed plausible range, it is still difficult to set the shape of prior distribution for each parameter due to the lack of sufficient information. Therefore, it is reasonable to consider that priors are uniformly distributed in the parameter space $\Re$ [46] as

$$p(\phi) = constant, \quad \phi \in \Re \tag{12}$$

and use a very informative initial guess for parameter vector in the Metropolis-Hastings algorithm to construct the Markov chain which will be discussed later.

3.3. Posterior

Plugging in prior (Eq. 12) and likelihood (Eq. 11) in the Bayes theorem (Eq. 6), the posterior can be found as

$$p(\phi|T_E) \propto \frac{I(\phi \in \Re)}{\sigma_1 \cdot \sigma_2 \cdot \ldots \cdot \sigma_n} exp\left\{-\frac{1}{2}\sum_{i=1}^{n}\frac{[T_{E,i} - T_{M,i}(\varphi)]^2}{\sigma_i^2}\right\} \tag{13}$$

The indicator function $I(\phi \in \Re)$ is used to check the bound of ϕ within the parameter space ($\Re$).

3.4. Markov chain Monte Carlo method

Markov chain Monte Carlo (MCMC) method is a well-established and flexible approach to numerically evaluate the posterior [40,46]. The key idea of MCMC method is to generate a sequence of dependent parameter values from a carefully constructed Markov chain by random walk through the parameter space ($\Re$). The walk starts with an arbitrary random value $\phi_j^{(0)}$ and continues through the parameter space by defining the move $\phi_j^{(K)} \rightarrow \phi_j^{(K+1)}$ with a transition density function ψ. In the Markov chain, there is an initial unstable transient phase (burn in period) which needs to be discarded to obtain limiting distribution. For the first time step, the initial guess for steam temperatures and heat transfer coefficients (h) are set to saturation temperature (corresponding to boiler pressure) and h values reported in Ref. [23], respectively. Since we have a very informative initial guess for the unknown parameters (i.e. steam temperature), we used a small burn-in period such as first $1,000$ MCMC steps and a small Markov chain of $10,000$ MCMC steps. To justify this, the Markov chains and the corresponding histograms are provided in Appendix A (for steam temperature at node $n2$) at three different time (10, 100, 1000 sec) after discarding the burn-in period. For the remaining time steps, the burn in period is neglected by setting estimated parameters of previous step as initial guess of current step i.e. $\phi_j^{(0)} = \phi_{j-1}^{(e)}$ where $\phi_{j-1}^{(e)}$ is estimated parameters at time step $(j-1)$. At any time, the parameter estimation is done by taking the mean of accepted samples of that parameter.

In the present study, the Metropolis-Hastings algorithm (Fig. 2) is used to sample the parameters to construct the Markov chain. The sampling begins with an initial parameter $\phi_j^{(0)}$. A candidate parameter ϕ_j^* for $\phi_j^{(K+1)}$ is sampled from the transition density function ψ. In this work, we define the transition density function ψ by a normal distribution with mean $\phi_j^{(K)}$ and variance of $\beta\,\phi_j^{(K)}$. This hyperparameter β determines the variance used in Metropolis-Hastings algorithm. Optimized value of this hyperparameter is estimated by a parametric study (not shown), and for this problem the optimized value of β is 0.025. The details of estimation process for this parameter are explained in our earlier work [29].

The candidate parameter ϕ_j^* can be randomly selected from the following distribution

$$\phi_j^* = \mathbb{N}\left(\phi_j^{(K)}, 0.025 \cdot \phi_j^{(K)}\right) \tag{14}$$

If the candidate parameter ϕ_j^* is outside of the parameter space ($\Re$), the indicator function $I(\phi \in \Re)$ becomes zero and the candidate parameter for this step is rejected directly. In contrast, if candidate parameter ϕ_j^* is within the parameter space ($\Re$), we accept this value with probability $\alpha(\phi_j^{(K)}, \phi_j^*)$ and set $\phi_j^{(K+1)} = \phi_j^*$ or reject this value with probability $1 - \alpha(\phi_j^{(K)}, \phi_j^*)$ and set $\phi_j^{(K+1)} = \phi_j^{(K)}$. Since the transition density function ψ is symmetric, the acceptance probability $\alpha(\phi_j^{(K)}, \phi_j^*)$ is defined as [46]

$$\alpha\left(\phi_j^{(K)}, \phi_j^*\right) = \min\left[r_N,\ a_r\right] \tag{15}$$

where acceptance ratio $a_r = \frac{p(\phi_j^*|T_E)}{p(\phi_j^{(K)}|T_E)}$ and r_N is a random number generated from uniform distribution with $(0, 1)$ interval. To evaluate the posterior probability distribution $p(\phi_j^*|T_E)$ and $p(\phi_j^{(K)}|T_E)$ for expression of a_r, we need to know the model results T_M in each MCMC iteration. Here, we used finite volume method (details are given in section 4.1) to obtain the model results from the corresponding forward problem. Once the a_r is determined, ϕ_j^* accepted or rejected based on the following criterion:

$$\phi_j^{(K+1)} = \begin{cases} \phi_j^{(K)}\ if\ a_r < r_N \\ \phi_j^*\ if\ a_r \geq r_N \end{cases} \tag{16}$$

For our problem, the parameter vector ϕ includes unknown physical parameters (φ), such as local steam temperatures T_{st}, local convective heat transfer coefficients h, as well as standard deviation (σ) of model error. In this work, we have considered two sets of convective heat transfer coefficients: one for the charging (from 0 to 580 sec) and the other for the discharging (from 580 sec towards the end). These two sets of local heat transfer coefficients are estimated based on the first 20 seconds of experimentally measured outer surface temperatures for both charging and discharging. Although heat transfer coefficients are varying locally, no temporal variation is considered during the charging or discharging process after the first 20 sec. Similar to heat transfer coefficients, the standard deviations for each spatial location are also estimated from the first 20 seconds of experimental measurements. Therefore, in the Metropolis-Hastings algorithm, the parameter vector ϕ is defined as

$$\phi = \begin{cases} T_{st,1}, T_{st,2}, ..., T_{st,n}, h_1, h_2, ..., h_n, \sigma_1, \sigma_2, ...\sigma_n\ for\ 0 < t \leq 20 \\ T_{st,1}, T_{st,2}, ..., T_{st,n}\ for\ 20 < t \leq 580 \\ T_{st,1}, T_{st,2}, ..., T_{st,n}, h_1, h_2, ..., h_n\ for\ 580 < t \leq 600 \\ T_{st,1}, T_{st,2}, ..., T_{st,n}\ for\ 600 < t \leq end \end{cases} \tag{17}$$

where the subscript numbers indicate the spatial location (along the circumferential direction) on the inner surface of the header. In our study, sufficiently large number of samples are obtained for each parameter, and the posterior mean (PM) of each parameter is used as point estimate of that parameter as

$$\hat{\phi}_{PM} = E(\phi|T_E) \tag{18}$$

We further smoothed out the point estimation by averaging over 20 seconds using a scheme similar to turbulent flow analysis. These estimated parameters are used to solve the governing transient heat conduction equation using a finite volume method (FVM).

Due to the complex nature of the physical heat transfer problem and use of the computationally intensive Markov chain Monte Carlo method, it took almost 2 weeks to complete all works presented in this study using a state-of-the-art desktop computer. Even though the proposed method is computationally expensive, the use of Bayesian inference over deterministic methods such as quasi-Newton, Gauss linearization or Gradient-based optimization methods is justified because the proposed Bayesian inference method considers sources of uncertainty available in the estimation process [46].

4. Results and discussions

4.1. Verification of FVM used for forward problem

As stated earlier, in each iteration of MCMC algorithm we need to know the model results from a forward problem. Thus, before estimating unknown parameters using the Bayesian inference framework, the accuracy of the numerical model used to solve the forward problem must be verified. In this study, the forward problem is an unsteady heat conduction in polar coordinate system, and we have developed an in-house finite volume code in R to solve the temperature distribution throughout the computational domain as shown in Fig. 1(b). Details about the numerical methods can be found in Refs. [47-49]. Briefly, the energy equation (Eq. 3) is discretized using central differencing scheme with $\Delta r = 1.04\ mm$ and $\Delta\theta = \pi/192$ (after performing grid independence study). For time marching, we have used an implicit scheme with time step of $\Delta t = 0.5\ sec$.

For verification, we have solved the forward problem with insulating boundary condition at the outer surface, while the inner surface was subjected to a Robin boundary condition. The inner surface heat transfer coefficient is varied, along the circumferential direction, as $h(\theta) = 1650 - 1350\cos(\theta)$ and the steam temperature is varied at a rate of $10^{\circ}C/min$ until it reaches its maximum at 150°C. The steam header is assumed to be at $T = 20^{\circ}C$ at the start of the heating process. Our numerical results are compared with the work of Duda [23], for identical initial and boundary conditions, where a finite element software, ANSYS, was used to calculate temperature distribution. The relative difference between our results and the results obtained by Duda is calculated for the first 1200 sec of simulation. The relative difference is less than 5%, as shown in Fig. 3, verifying our in-house numerical model for the heat conduction problems with transient boundary conditions. The relatively small variation might be from the fundamental differences in schemes used for these two numerical formulations (finite volume vs finite element method). Moreover, the interpolation method used to find the temperature dependent material properties (C_p , k) might also lead to differences in temperature results with Ref. [23].

4.2. Outer surface temperature: forward model vs Bayesian model

Once the outer surface temperatures are calculated using the FVM, they are used as experimental temperatures in the inverse problem to estimate the steam temperature and convective heat transfer coefficients. The results from our reverse problem are presented in Fig. 4 along with the known values from the forward problem (aka experiment). Our predicted parameters are in very good agreement with known parameters (steam temperature and local heat transfer coefficient). These predicted parameters successfully reproduced the outer surface temperature of header, as shown in Fig. 5, verifying our Bayesian algorithm for reverse problem. We also studied the effects of measurement error in estimated parameters to establish the robustness of the proposed algorithm. Similar to Ref. [23], we have introduced an error in the outer surface temperatures with zero mean and a prescribed standard deviation. The standard deviation for this test is $1/12^{\text{th}}$ of the outer surface temperatures obtained from the forward problem described earlier. The inverse problem is solved for steam temperature and heat transfer coefficients, and the results are presented in Fig. 6. Albeit, due to an increase in measurement error, there are higher uncertainties in the estimated parameters (steam temperatures and local convective heat transfer coefficients). However, we found a very good agreement for the outer surface temperatures as shown in Fig. 7. Nonetheless, with additional experimental uncertainties, our Bayesian model can still capture the similar results for steam temperatures and heat transfer coefficients, as in Fig. 4, demonstrating the stability of the algorithm.

Table 1
Model error between measured temperatures and corresponding prediction.

Nodes, i	σ_i (Mean ± SD)
O1	4.98 ± 2.39
O2	5.04 ± 2.32
O3	4.91 ± 1.80
O4	5.42 ± 1.20
O5	6.07 ± 0.37
O6	6.27 ± 0.91
O7	4.91 ± 2.82
O8	3.30 ± 2.40
O9	2.82 ± 0.53
O10	1.51 ± 1.00
O11	2.27 ± 0.55
O12	1.83 ± 0.26
O13	1.31 ± 0.11

4.3. Estimated parameters

We have used the Bayesian approach described in section 3 to determine the unknown parameters of the current problem. For this problem, the unknown parameters include physical parameters such as steam temperature T_{st}, convective heat transfer coefficients h at the inner wall and inner surface temperatures T_i, as well as standard deviations σ of model error. Since the inner surface temperature can be obtained from the analysis of boundary condition, we reduced the number of unknown quantities by excluding inner surface temperature from the parameter vector. Therefore, we need to determine two sets of physical parameters: T_{st}, h and one set of model error, σ. These unknown parameters are estimated by Bayesian method where we have used the experimental data (outer surface temperature) given in Ref. [23] as evidence.

Model error, σ: The model error (σ) measures the difference between experimentally measured temperature and corresponding model prediction. In this work, the model error is calculated for 13 measurement points on the outer surface of the header (Table 1). In Bayesian approach, these model errors are estimated as a distribution instead of point estimate. Although all of these 13 values are not normally distributed, for simplicity, we represented these values as mean ± SD (standard deviation) similar to normal distribution. As represented in Table 1, the mean model errors are larger for points located in the lower part of the header. This implies that the differences between the modeled temperatures and measured temperatures are also larger for points located in the lower part of the header.

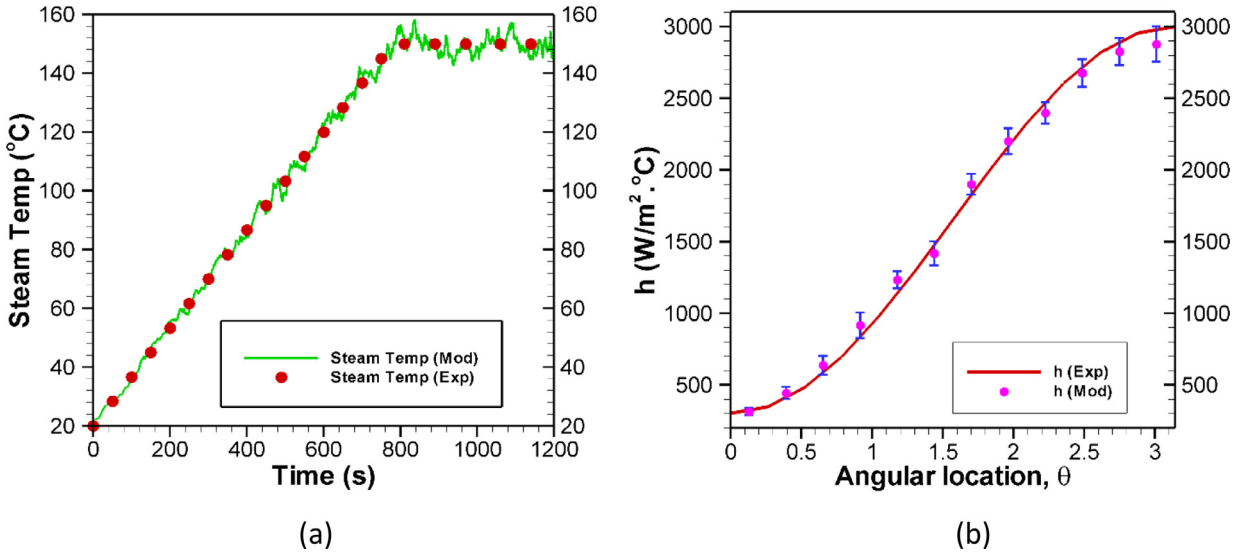

Fig. 4. Estimated parameters for numerical verification of the Bayesian inference. (a) Comparison of the (a) steam temperature and (b) heat transfer coefficient, *h*, between known values that are obtained from the forward model (Exp) and modeled results (Mod).

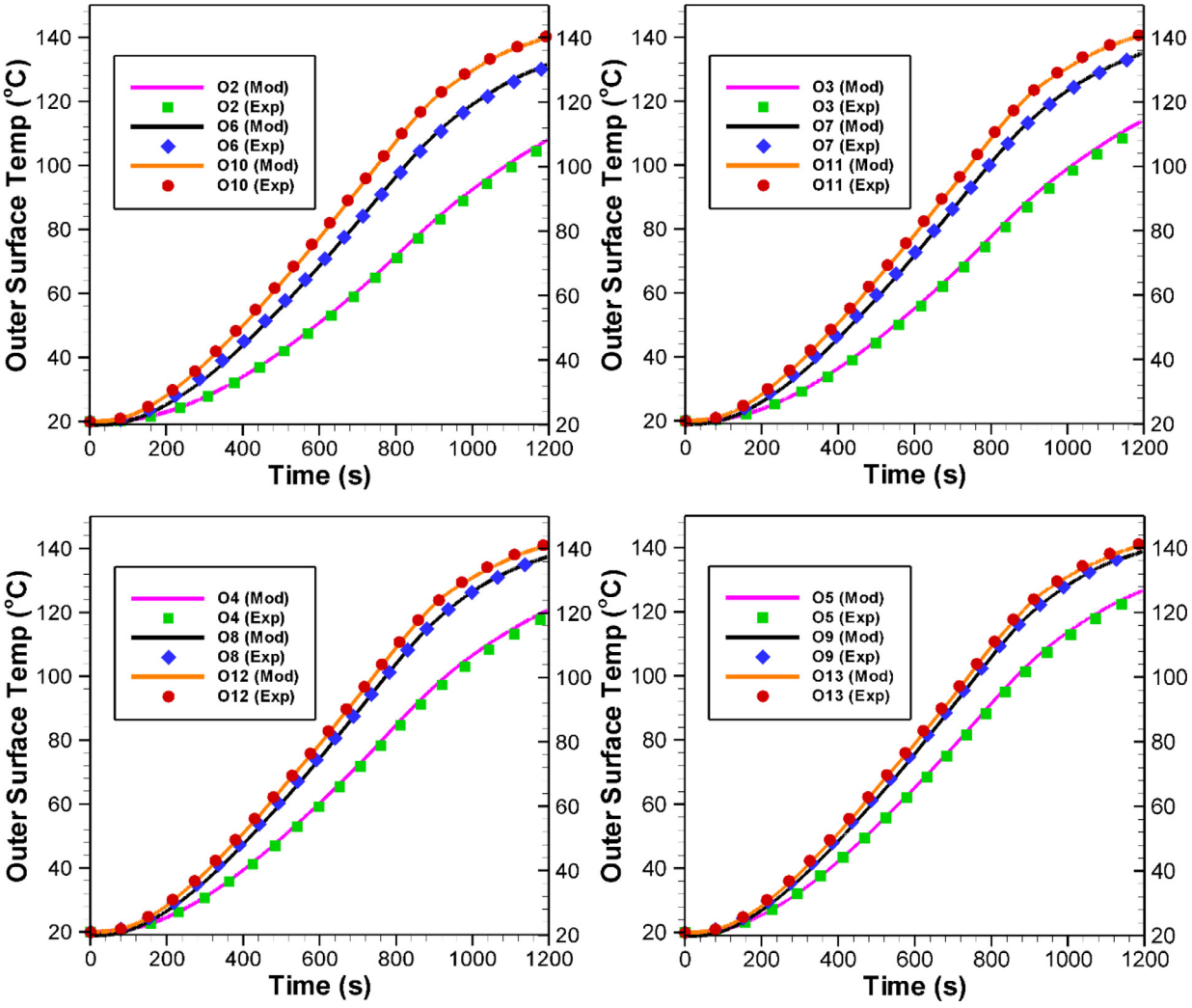

Fig. 5. Comparison of the outer surface temperature between experimental (calculated using the FVM) measurements (Exp) and Bayesian model (Mod).

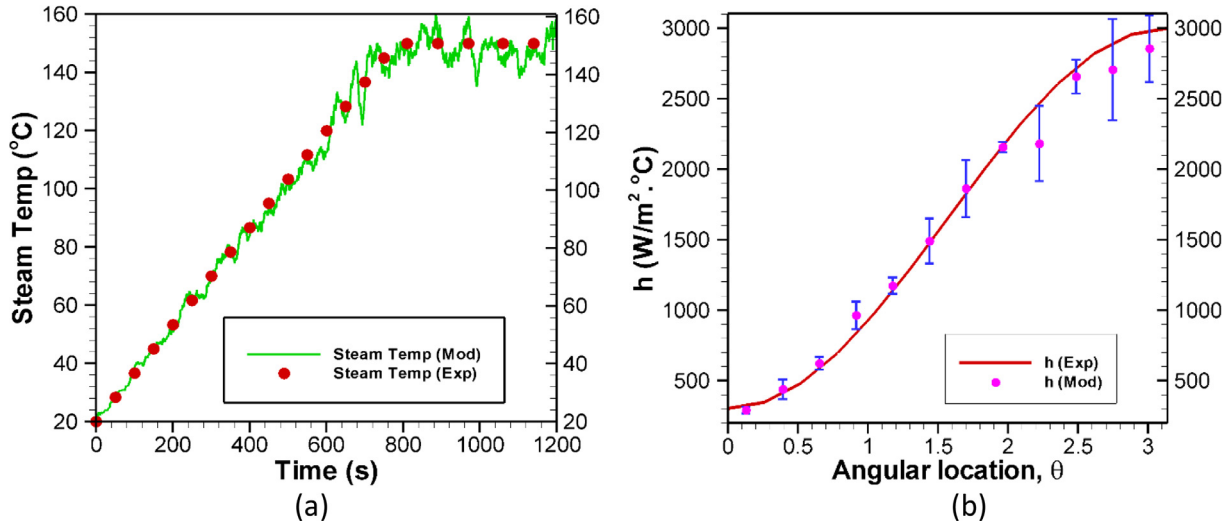

Fig. 6. Estimated parameters with added errors. Comparison of the (a) steam temperature and (b) heat transfer coefficient, h, between known values obtained from the forward model (Exp) and Bayesian model (Mod). The error bar is given as $mean \pm 3SD$.

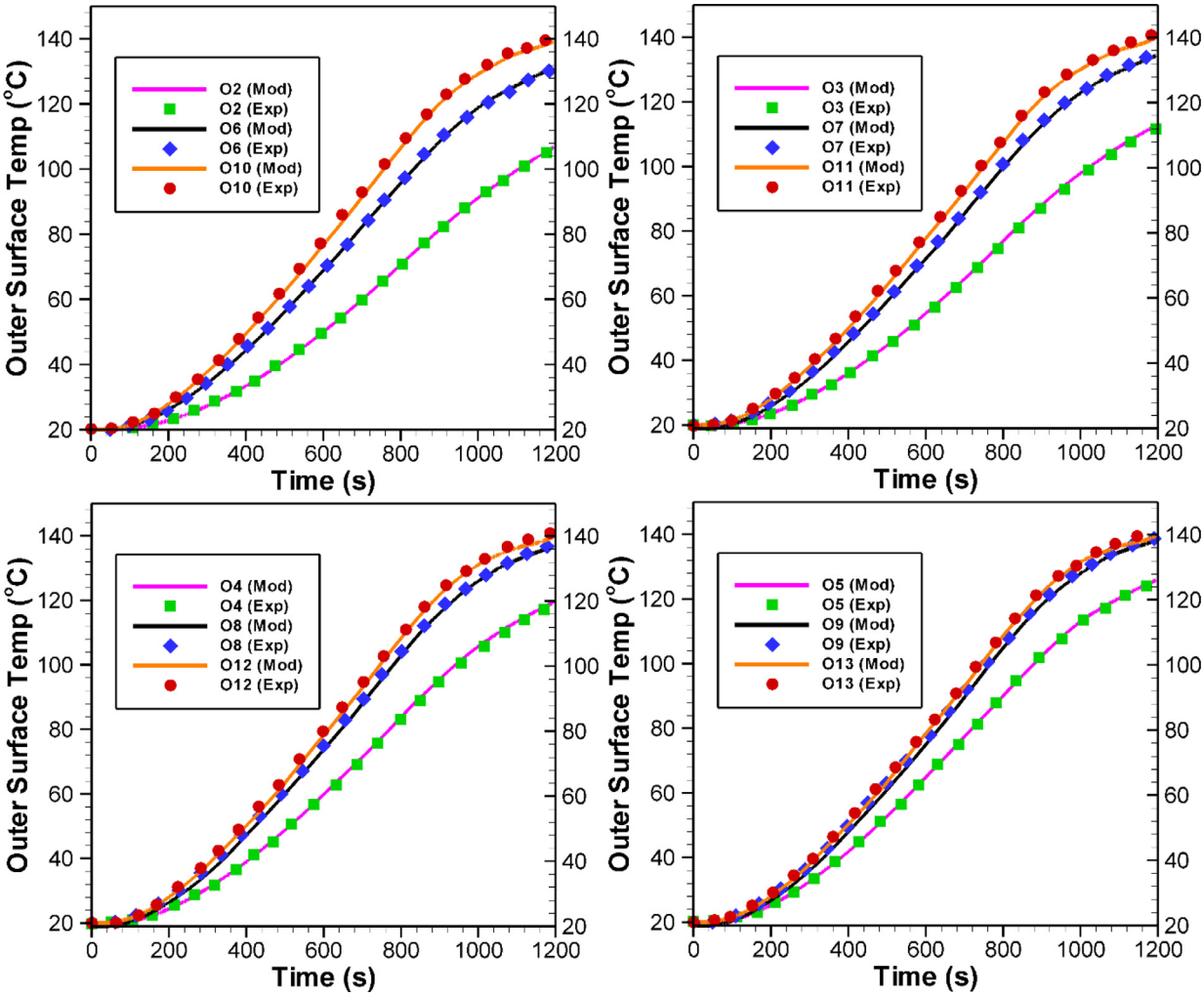

Fig. 7. Comparison of the outer surface temperature between experimental (calculated using the FVM) measurements (Exp) with added measurement errors and modeled results (Mod).

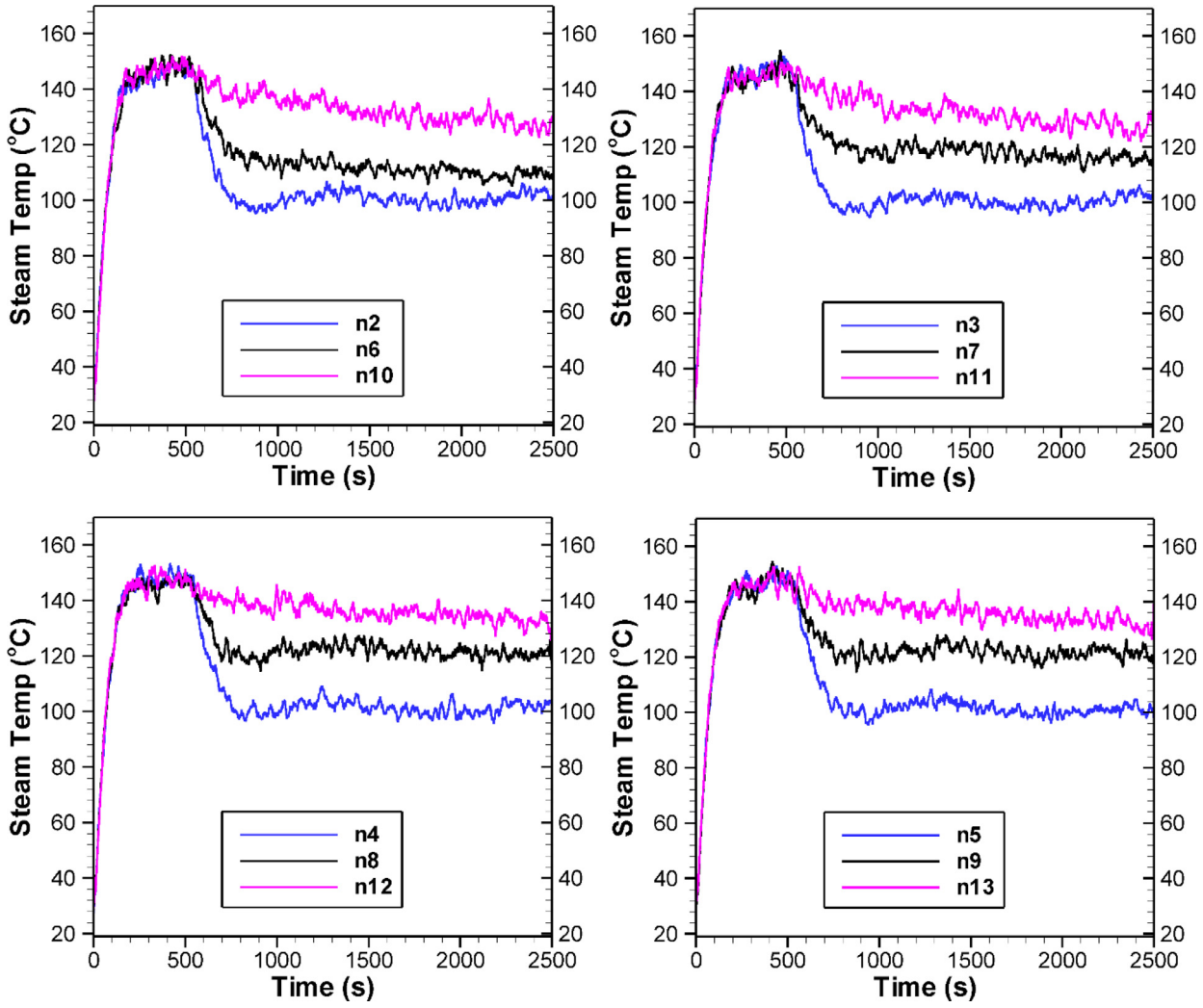

Fig. 8. Estimated transient steam temperature at different locations on the inner surface of the steam header. The temperature profiles for different nodes maintain a similar trend while rising (charging process, for $t \leq 580$ sec) but later (discharging process, for $t > 580$ sec) significant differences are visible among them. Though condensation of steam occurs all along, its effect is visible only when the exit valve is open which explains the noticeable difference in the temperature profiles beyond 580 sec. *The zigzag in the steam temperature estimation is due to stochastic nature of Bayesian inference.*

Steam temperature, T_{st}: Fluid temperature at the inner side of a steam header is inaccessible, and the Bayesian technique provides an opportunity to estimate them. Fig. 8 presents the transient steam temperatures next to the 12 inner nodes ($n2$, $n3$, ..., $n13$) calculated using the Bayesian inference framework. For better presentation of the results, these 12 nodes are divided into four groups: first group (nodes $n2$, $n6$ and $n10$), second group (nodes $n3$, $n7$, and $n11$), third group (nodes $n4$, $n8$ and $n12$) and fourth group (nodes $n5$, $n9$, and $n13$). The predicted results show that the steam temperature inside the header rises at first and after reaching a peak, it starts to decrease. It is due to the fact that the steam is supplied into the header for 580 sec before opening the exit valve. Although the rise in steam temperature for all the nodes follow almost the same trend, it is not the case when the temperature starts decreasing during the discharge process. This is because of two different types of flow as well as associated heat transfer mechanism. For instance, during the charging process, the pressure inside the chamber keeps rising and thus the temperature of the steam as well as condensed water inside the header rises. Though condensation starts occurring from the beginning, its effect is not visible as steam keeps on coming during the charging process. Since the water stays at the same temperature as the steam, the rise in temperature is same for all the nodes up to 580 sec. However, when the exit valve is open, the steam and the condensed water (at the bottom half) have different temperatures which is reflected by their significantly different temperature profiles. We also observed fluctuations in fluid temperature at all nodal points, which is a signature of Bayesian inference technique.

Heat transfer coefficient, h: Another parameter that impacts the heat transfer through the thick header wall is the convective heat transfer coefficient, h. Using the Bayesian inference technique, the local heat transfer coefficients of the inner fluid are estimated based on the measured temperatures at the outer surface of the header. Since the flow condition changes with time during the entire experiment, two different values of heat transfer coefficient are estimated for each node: one is for the charging process ($t \leq 580\ sec$) and the other is for discharging process ($t > 580\ sec$) assuming that the heat transfer coefficients remain constant during each process. The estimated heat transfer coefficient values for the 12 inner nodes are provided in Table 2 for both heating (charging) and cooling (discharging) process. For heating process, the lowest heat transfer coefficient is observed for node $n2$ and the highest heat transfer coefficient is observed for node $n13$. A similar trend

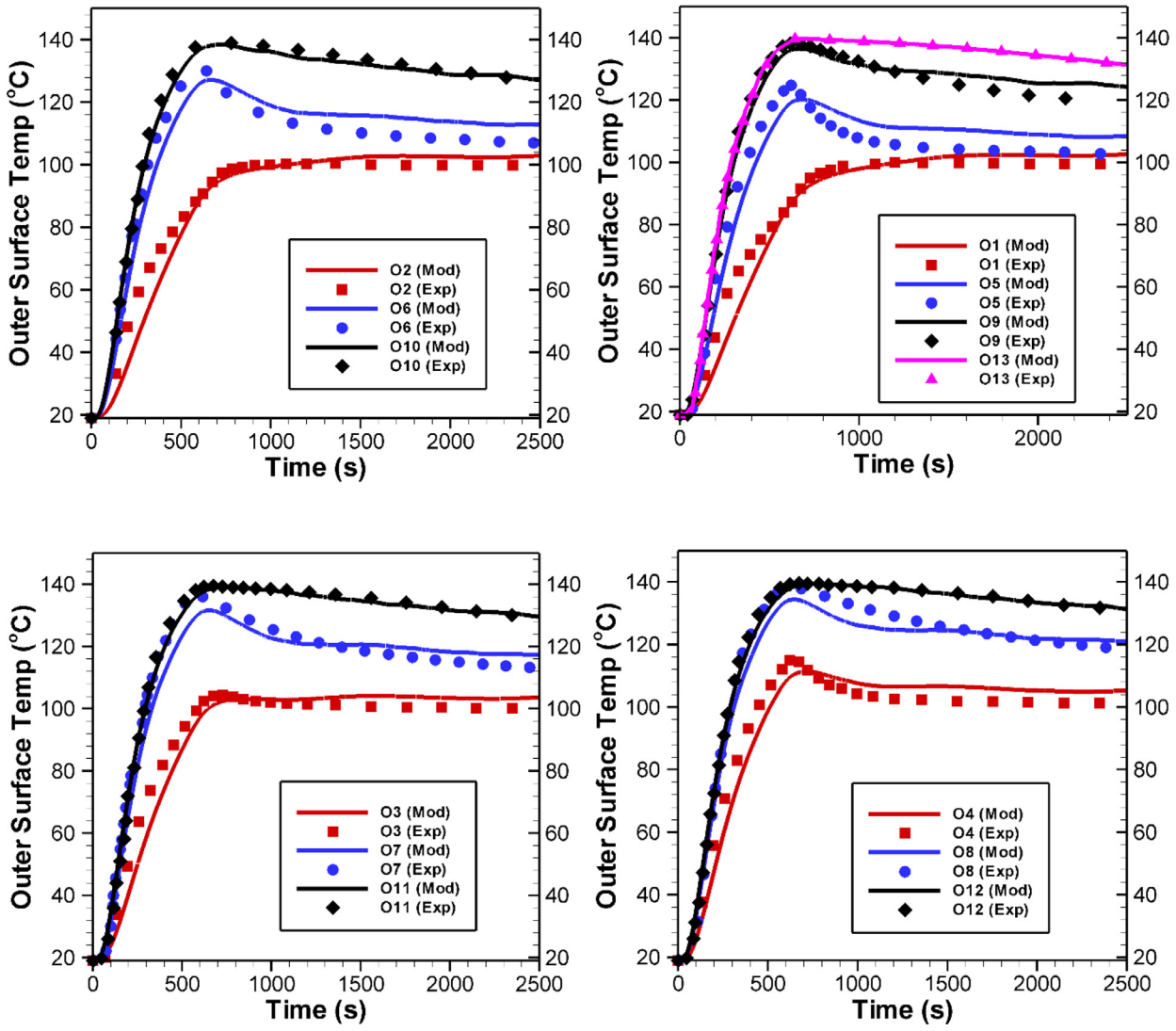

Fig. 9. Comparison of the outer surface temperature between experimental measurements (Exp) and modeled results (Mod). The solid lines represent the temperature profiles obtained by finite volume method with estimated parameters and the symbols represents the experimental observations. The modeled results are in good agreement with the experimental measurements.

Table 2
Estimated heat transfer coefficients near the inner surface of the steam header.

Nodes, i	Heat Transfer Coefficients, h_i ($W/m^2.°C$) (Mean ± SD)	
	Charging Process ($t \leq 580$ sec)	Discharging Process ($t > 580$ sec)
$n2$	349.79 ± 16.08	280.31 ± 10.07
$n3$	408.66 ± 38.48	319.88 ± 34.76
$n4$	805.07 ± 53.43	614.13 ± 41.97
$n5$	1166.45 ± 125.29	983.85 ± 50.09
$n6$	1910.45 ± 137.53	1264.98 ± 127.17
$n7$	3573.76 ± 142.50	3228.45 ± 146.78
$n8$	4702.63 ± 137.83	3524.33 ± 264.57
$n9$	6033.40 ± 204.94	3502.40 ± 498.23
$n10$	6180.13 ± 692.91	4073.91 ± 257.87
$n11$	7862.06 ± 553.85	2828.29 ± 1437.31
$n12$	8134.08 ± 632.43	2541.56 ± 1798.65
$n13$	10073.99 ± 1577.80	6856.51 ± 634.38

is noticed for the cooling process as well. However, both the highest and lowest values of the heat transfer coefficient for the cooling process are significantly lower (~20 to 30%) than their heating counter parts. This is because of the different flow conditions during heating and cooling process.

It is also evident that the nodes located at the upper half of the inner surface ($n8 - n13$) have remarkably higher values of heat transfer coefficients than the nodes at the lower half ($n2 - n7$). At the upper nodes, due to the presence of hot steam, heat transfer coefficients tend to be higher, which means that heat is being transferred more rapidly. On the other hand, the opposite scenario is observed at the lower nodes, due to the presence of condensed water which indicates a slower rate of heat transfer. Due to phase change inside the header, there is an order of magnitude variation in heat transfer coefficients along the spatial location.

4.4. Validation of Bayesian inference

Once the unknown physical parameters, T_{st} and h, are estimated, the efficacy of the proposed Bayesian approach is demonstrated by comparing the calculated temperature profiles at the outer surface of header with the experimental measurements from Ref. [23]. Fig. 9 shows the comparison between modelled and ex-

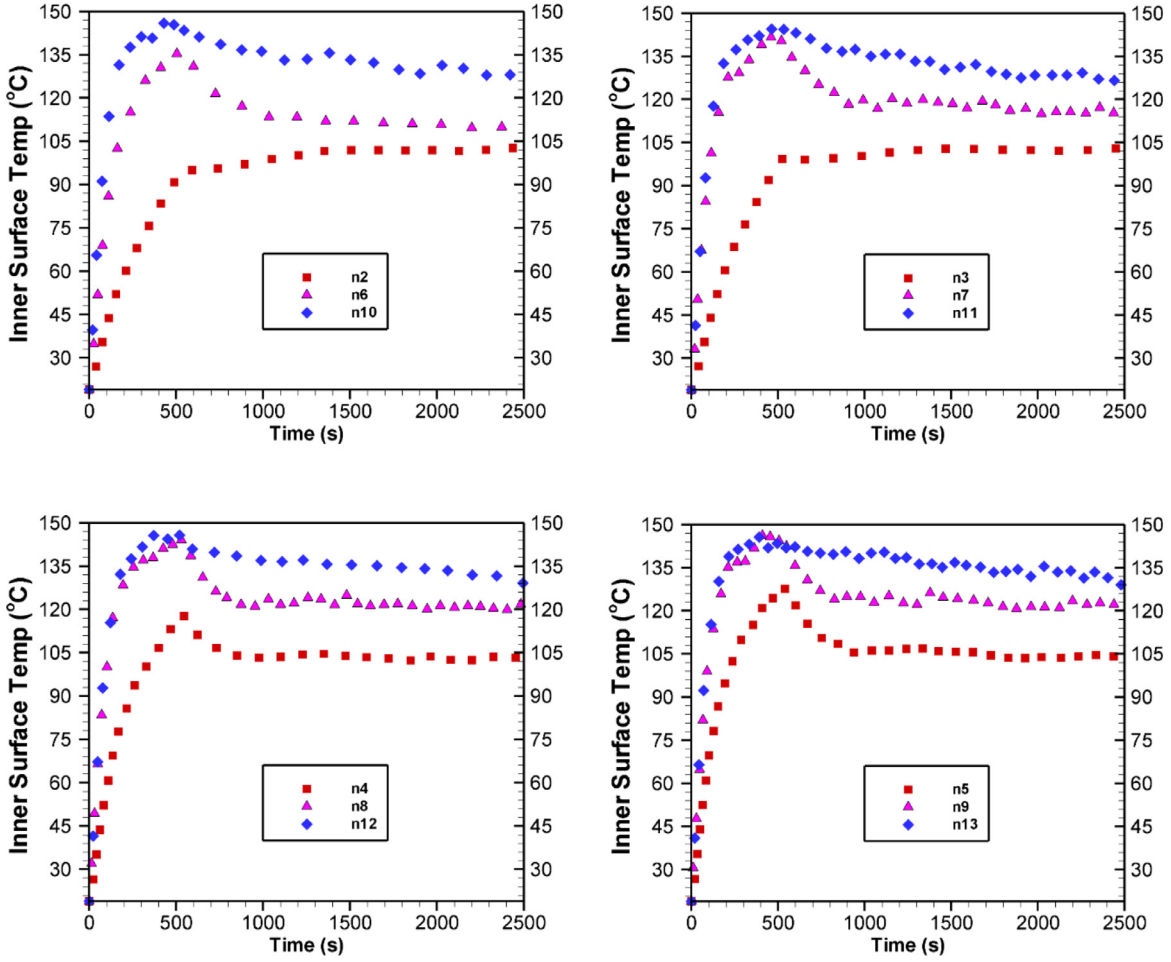

Fig. 10. Predicted inner surface temperature profiles of the steam header with time at different locations. For maintaining clarity and better visibility, the profiles are divided into four different panels where the adjacent nodes are not shown in the same plot. The nodes located at the upper half maintain a significantly higher temperature profile than its bottom counterpart throughout the entire time span.

perimentally measured temperatures. Here the solid lines indicate the results from solving forward problem with estimated parameters (Mod) and the symbols represent the results obtained from the experiments (Exp) [23]. As mentioned earlier, the experimental measurements were taken on the 13 nodes of the steam header at its outer surface. Thus, the modeled temperatures are also calculated on the same 13 nodes. For illustration purpose, results from these 13 nodes were divided into four groups.

Although there are some differences between modeled and measured temperatures, as shown in Fig. 9, it is evident that the overall model results are very close to experimental measurements with small relative error. Interestingly, the modeled results exhibit both undershooting (a little bit lower than experimental temperature) and overshooting (a little bit higher than experimental temperature) behavior because Bayesian inference assumed an error with zero mean. For instance, the model temperatures seem to undershoot during the heating process and then starts to overshoot during the cooling process especially in the lower half of the steam header, though prediction is pretty close to experimentally observed values for upper half. The noticeable variation in the lower half is due to complex heat transfer phenomenon, such as phase change from steam to water along with accumulation of condensate from other parts of the header. These complex heat transfer mechanisms suggest that the heat transfer coefficient at a particular nodal point varies with time during the charging or discharging process. Since we assumed a constant heat transfer coefficient at a particular location throughout the charging or discharging process, we were not able to capture these discrepancies in the lower half of the header. A transient heat transfer coefficient (similar to steam temperatures) may reduce the discrepancies between modeled and experimental temperatures at the lower nodal points. But this will be computationally prohibitive since number of Markov chains will increase by 5000 times for a 2500 sec computation. Nevertheless, the current Bayesian model can capture the unknown steam temperatures and heat transfer coefficients, as well as complex heat transfer phenomena occurring inside the steam header.

4.5. Inner surface temperature

Once the steam temperature, T_{st} and the heat transfer coefficient, h are estimated by the Bayesian inference, the inner surface temperatures can be calculated by solving the forward problem using finite volume method. The calculated inner surface temperatures, T_i are provided in Fig. 10 and presented in a way like Fig. 8 for better illustration. Similar to the steam temperature, the inner surface temperature first rises rapidly after coming in contact with the hot steam and reaches peak at around 580 sec. After that the temperature profile either flattens or starts to decrease. Also,

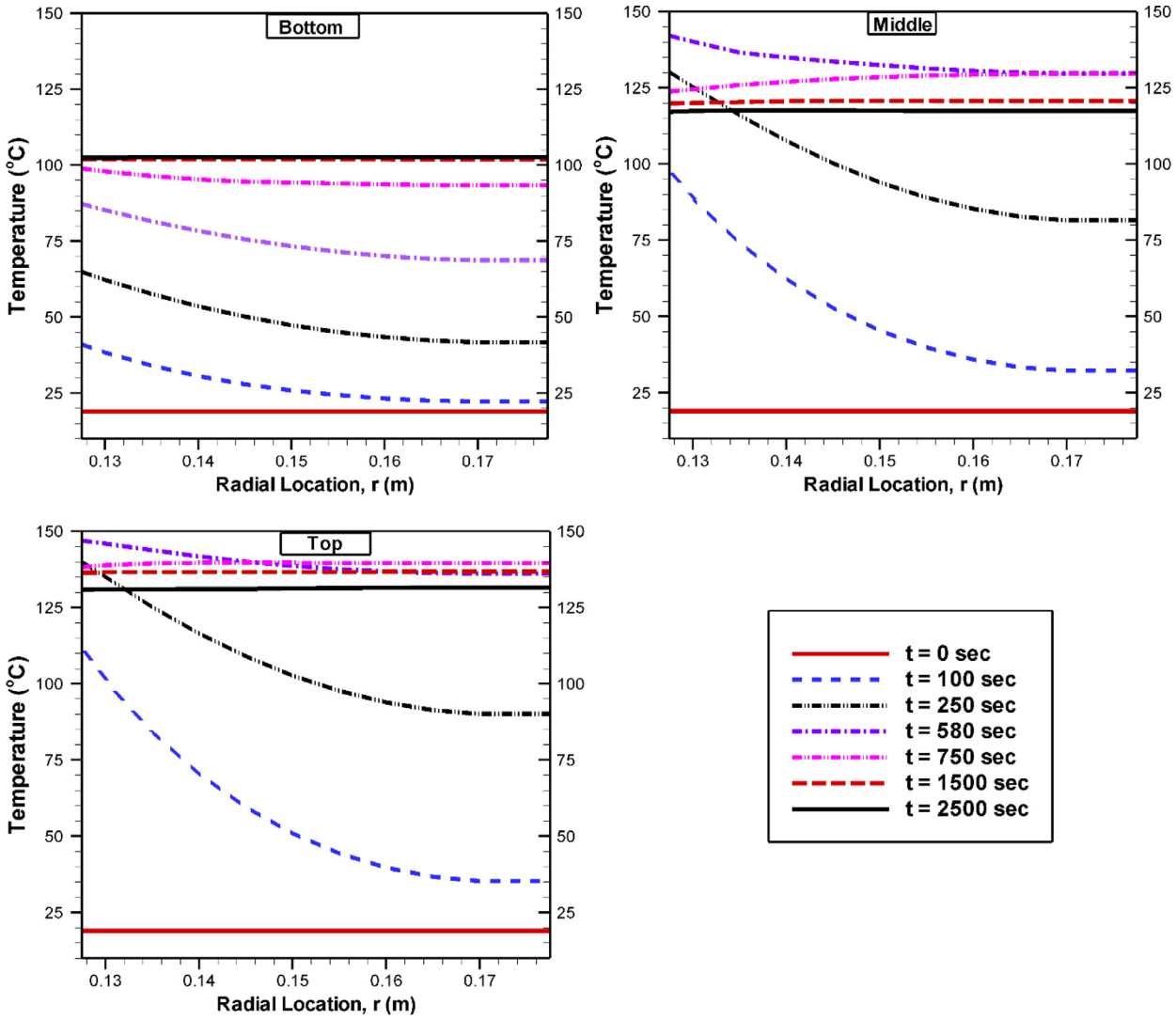

Fig. 11. Temperature distribution along the radial direction at bottom, middle and top part of the header at various times.

the T_i at lower node points are consistently lower than the upper node points. For instance, the nodes at the lower part of the header achieve the peak values around the temperature range of 90 to 130°C and finally come down to approximately 105°C. On the other hand, the nodes at the upper part achieve the peak around 148°C and finally come down to approximately 127°C. Middle nodes show identical behavior as the upper nodes for ($t \leq 580$ sec), but their values are bounded by the upper and lower domain during the cooling phase.

The reason for the difference in inner surface temperature profiles can be described in a way similar to that of steam temperature. As stated earlier, the saturated steam (@ 10 bar) is continuously supplied into the chamber for 580 sec by keeping the exit valve closed. Due to high pressure inside the chamber, the steam is condensed at this temperature and starts being converted into water. But due to the influence of gravity, condensed steam largely settles down at the bottom and thus the lower nodes always seem to maintain lower temperatures. Due to this condensation effect, nodes ($n1 - n6$) don't reach a temperature value higher than 135°C, but the nodes ($n7 - n13$) reach temperature values as high as 148°C which is very close to the steam temperature peak (150°C) as shown in Fig. 8.

4.6. Radial distribution of temperature

The temperature distribution in the radial direction is shown in Fig. 11 for three selected angular locations: $\theta = -82.5°$, 0 and 82.5° representing bottom, middle and top, respectively. At the beginning ($t =$ 50, 150, 250 and 375 sec), the inner surface ($r = r_i$) has higher temperature because heat is transferred from steam to header through convective heat transfer mechanism. During the charging process, the temperatures gradually decrease from inner surface to outer surface, and finally become flat because of insulating boundary condition at the outer surface. The decrease of temperatures in radial direction is steeper at upper half than the middle or lower half. For all three angular positions, the highest temperature keeps increasing at the inner surface with time until the opening of the exit valve at $t =$ 580 sec. Afterwards, the temperature profiles are different depending on the value of θ. For instance, at the top ($\theta = 82.5°$), the profiles flatten out, which indicates that the inner and outer surface gradually reach the same temperature due to insulating boundary condition. However, for the bottom and middle portion ($\theta = -82.5°$ and 0, respectively), a slightly increasing trend is visible. This occurs because, at these locations, the inner surface temperatures don't rise as much

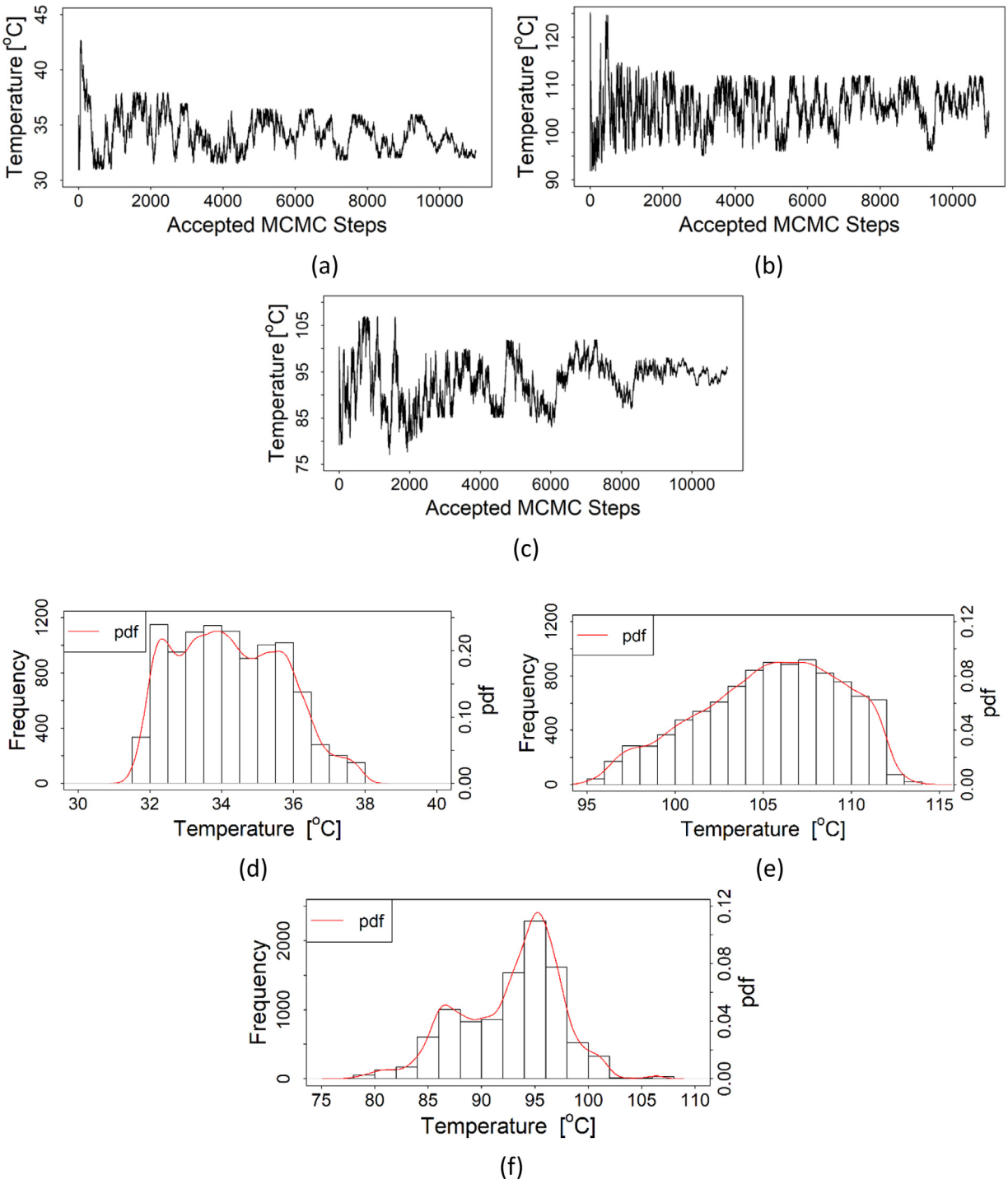

Fig. A1. Markov chains for steam temperature for node *n*2 at different times: (a) 10 sec, (b) 100 sec, and (c) 1000 sec. The corresponding histograms (after discarding the burn-in states) are given in (d), (e) and (f) respectively.

due to the presence of water and thus, heat transfer is directed from the outer surface to the inner surface and then to the inner fluid.

5. Conclusions

Often in real life, while tackling physical problems, a situation arises when it is either impossible or extremely difficult to extract information from a location that is not physically reachable. For such a situation, the Bayesian inference technique can be a tremendously helpful tool that can solve the problem from an entirely different perspective. In this study, a Bayesian inference framework is proposed based on the Markov chain Monte Carlo method to predict the steam temperatures and heat transfer coefficients at the inner side of a steam header.

The physical problem discussed in this work was based on the transient heat conduction through a steam header wall for which the parameters at the inner surface are estimated depending on

the information available for the outer surface. The model, after rigorous validation, is able to successfully estimate the transient temperature profiles of the supplied steam and clearly exhibited the difference in its behavior for the top and bottom half of the header. Due to the existence of two processes- charging and discharging, the convective heat transfer coefficient is estimated to be different which properly captures the differences between the two parts of heat transfer. Finally, the estimated steam temperature and the heat transfer coefficient are used to calculate the inner surface temperature of the header that also exhibited a difference between temperature profiles at the top and bottom half of the header. The variations of temperature profiles along the inner surface are mainly caused by the condensation of steam and its accumulation at the lower part due to gravity. The estimated steam temperature and the heat transfer coefficient are also used to predict the experimental measurements (surface temperature) on the outer surface. We observed correlated discrepancies in outer surface temperature since we updated all parameters at the same time during the Markov chain formation through Metropolis-Hastings algorithm. Single parameter modification in each step of Metropolis-Hastings algorithm (as described in ref [31]) may reduce the correlated residuals between modeled and experimental temperatures. However, this will increase the computational time significantly since we have estimated a very large number of parameters in this complex heat transfer problem.

The presented Bayesian method can be applied for reducing the heat loss during the power block's start-up and shut-down operations via optimization which may enhance the power block's durability. The Bayesian framework can be further extended for more complicated systems such as conventional as well as nuclear power plants.

Declaration of Competing Interest

The authors declare that they have no known competing financial interests or personal relationships that could have appeared to influence the work reported in this paper.

Author contribution statement

Aminul Islam Khan: Methodology - Bayesian Inference, Formal analysis, Validation, Visualization, Writing - Original draft & editing. **Md Muhtasim Billah**: Methodology - Finite Volume Analysis, Visualization, Writing - Original draft & editing. **Chunhua Ying**: Methodology - Finite Volume Analysis, Data Curation, Visualization. **Jin Liu**: Writing - Review & Editing. **Prashanta Dutta**: Conceptualization, Supervision, Writing - Review & Editing.

Appendix A. Markov chains and histograms for node *n*2 at different time points

Usually, a very large number is considered as burn-in period for Markov chains but, for this study, only 1000 MC steps have been used (as depicted in section 3.4). For example, in our earlier work [29] or the study carried out by Choi et al. [46], 5×10^4 burn-in states were used. However, the use of very small burn-in states in this problem is justified as we have used very narrow, well-educated range for the unknown parameters. Essentially, we have created a Markov chain for steam temperatures at every time point. Therefore, for steam temperature at any spatial point, the number of Markov chains is equal to the number of time steps used in our model. On the other hand, we have considered the convective heat transfer coefficient as a two-step constant. Thus, for convective heat transfer coefficient at any spatial point, we have only two Markov chains. For steam temperature at node *n*2, the Markov chains are presented at different time steps in Fig. A1. For brevity, only one of the estimated parameters are shown at node *n*2, though the behavior is similar for other nodes and/or variables. As shown in Fig. A1. ((a), (b), (c)), within 11000 MCMC accepted steps, temperatures converged to a well distributed Markov chain. The corresponding histograms after discarding the burn-in states are also shown in Fig. A1. ((d), (e), (f)). Since we used $1,000$ data points as burn-in states, $10,000$ states have been used in the posterior Markov chains. As shown in Fig. A1, some posteriors yield a normal distribution, whereas others exhibit the behavior of a gamma distribution with longer tail either at the lower or upper end. These results indicate that use of very small burn-in states and/or limited number of accepted MCMC steps are adequate for this problem.

References

[1] A. Gelman, in: Bayesian data analysis, second ed., Chapman & Hall/CRC, Boca Raton, FL, 2004, pp. 1–663.
[2] R.J. Ritchie, T. Prvan, Current statistical methods for estimating the K-m and V-max of Michaelis-Menten kinetics, Biochem Educ 24 (4) (1996) 196–206.
[3] B.P. Bezruchko, D.A. Smirnov, Extracting knowledge from time teries: An introduction to nonlinear empirical modeling, Springer Ser Synerg, Russia (2010) 1–405.
[4] E. Baake, M. Baake, H.G. Bock, K.M. Briggs, Fitting ordinary differential-equations to chaotic data, Phys Rev A 45 (8) (1992) 5524–5529.
[5] M. Peifer, J. Timmer, Parameter estimation in ordinary differential equations for biochemical processes using the method of multiple shooting, IET Syst Biol 1 (2) (2007) 78–88.
[6] M.D. Collins, W.A. Kuperman, Inverse problems in ocean acoustics, Inverse Probl 10 (5) (1994) 1023–1040.
[7] D.P. Knobles, M. Gray, R.A. Koch, A. Cook, in: Acoustic sensing techniques for the shallow water environment: inversion methods and experiments, first ed., Springer, 2006, pp. 321–328.
[8] W.C. Thacker, Oceanographic inverse problems, Physica D 60 (1-4) (1992) 16–37.
[9] C. Wunsch, in: The ocean circulation inverse problem, Cambridge University Press, Cambridge; New York, 1996, pp. 1–442.
[10] Y.Z. Xu, Inverse acoustic scattering problems in ocean environments, J Comput Acoust 7 (2) (1999) 111–132.
[11] A.V. Akhmetzyanov, A.M. Salnikov, Methods and algorithms for the solution of inverse problems of modelling and control in reservoir engineering, IFAC Papers OnLine 48 (3) (2015) 1259–1263.
[12] O. Dorn, R. Villegas, History matching of petroleum reservoirs using a level set technique, Inverse Probl 24 (3) (2008).
[13] P. Tahmasebi, F. Javadpour, M. Sahimi, Stochastic shale permeability matching: Three-dimensional characterization and modeling, Int J Coal Geol 165 (2016) 231–242.
[14] S.X. Huang, J. Xiang, H.D. Du, X.Q. Cao, Inverse problems in atmospheric science and their application, J Phys Conf Ser 12 (2005) 45–57.
[15] M. Ferraresi, E. Todini, R. Vignoli, A solution to the inverse problem in groundwater hydrology based on Kalman filtering, J Hydrol 175 (1-4) (1996) 567–581.
[16] D. O'Malley, An approach to quantum-computational hydrologic inverse analysis, Sci Rep-UK 8 (2018).
[17] Y. Censor, A. Segal, Iterative projection methods in biomedical inverse problems, Crm Ser 7 (2008) 65–96.
[18] M.A. Hussain, B. Noble, B. Becker, Computer-simulation of an inverse problem for electric-current computed-tomography using a uniform triangular discretization, P IEE Embs 11 (1989) 448–450.
[19] P.V. Konarev, F.N. Chukhovskii, V.V. Volkov, To the solution of the inverse problem of X-Ray topo-tomography. computer algorithms and 3D reconstruction on the example of a crystal with a point defect of Coulomb type, Crystallogr Rep 64 (2) (2019) 191–200.
[20] F. Martelli, S. Del Bianco, G. Zaccanti, Inverse problem for biomedical applications: use of prior information on target and forward model parameters, Proc Spie (2011) 7896.
[21] W. Choi, R. Ooka, Interpretation of disturbed data in thermal response tests using the infinite line source model and numerical parameter estimation method, Appl Energ 148 (2015) 476–488.
[22] O. Strebel, A preprocessing method for parameter estimation in ordinary differential equations, Chaos Soliton & Fract 57 (2013) 93–104.
[23] P. Duda, Numerical and experimental verification of two methods for solving an inverse heat conduction problem, Int J Heat Mass Tran 84 (2015) 1101–1112.
[24] V. Dua, An artificial neural network approximation based decomposition approach for parameter estimation of system of ordinary differential equations, Comput Chem Eng 35 (3) (2011) 545–553.
[25] A.I. Khan, Q. Lu, D. Du, Y.H. Lin, P. Dutta, Quantification of kinetic rate constants for transcytosis of polymeric nanoparticle through blood-brain barrier, BBA-Gen Subjects (12) (2018) 2779–2787 1862.
[26] M. Raissi, P. Perdikaris, G.E. Karniadakis, Physics informed deep learning (part II): Data-driven discovery of nonlinear partial differential equations, Colorado (2017) 1–19.

[27] M. Raissi, P. Perdikaris, G.E. Karniadakis, Physics informed deep learning (part I): Data-driven solutions of nonlinear partial differential equations, Colorado (2017) 1–21.
[28] C.L. Bremer, D.T. Kaplan, Markov chain Monte Carlo estimation of nonlinear dynamics from time series, Physica D-Nonlinear Phenomena 160 (1-2) (2001) 116–126.
[29] A.I. Khan, J. Liu, P. Dutta, Bayesian inference for parameter estimation in lactoferrin-mediated iron transport across blood-brain barrier, Biochim Biophys Acta Gen Subj 1864 (3) (2020) 129459.
[30] M.D. Robinson, D.J. McCarthy, G.K. Smyth, edgeR: a bioconductor package for differential expression analysis of digital gene expression data, Bioinformatics 26 (1) (2010) 139–140.
[31] E.P. Campbell, D.R. Fox, B.C. Bates, A Bayesian approach to parameter estimation and pooling in nonlinear flood event models, Water Resour Res 35 (1) (1999) 211–220.
[32] F.C. Coelho, C.T. Codeco, M.G.M. Gomes, A Bayesian framework for parameter estimation in dynamical models, PLOS One 6 (5) (2011).
[33] M. Girolami, Bayesian inference for differential equations, Theor Comput Sci 408 (1) (2008) 4–16.
[34] Y.X. Huang, D.C. Liu, H.L. Wu, Hierarchical Bayesian methods for estimation of parameters in a longitudinal HIV dynamic system, Biometrics 62 (2) (2006) 413–423.
[35] T.H. Duan, Auto regressive dynamic Bayesian network and its application in stock market inference, Ifip Adv Inf Comm Te 475 (2016) 419–428.
[36] M. Maragoudakis, D. Serpanos, Exploiting financial news and social media opinions for stock market analysis using MCMC Bayesian inference, Comput Econ 47 (4) (2016) 589–622.
[37] D. van Ravenzwaaij, P. Cassey, S.D Brown, A simple introduction to Markov Chain Monte-Carlo sampling, Psychon Bull Rev 25 (1) (2018) 143–154.
[38] J.M. Toivanen, V. Kolehmainen, T. Tarvainen, H.R.B. Orlande, J.P. Kaipio, Simultaneous estimation of spatially distributed thermal conductivity, heat capacity and surface heat transfer coefficient in thermal tomography, Int J Heat Mass Tran 55 (25-26) (2012) 7958–7968.
[39] S. Parthasarathy, C. Balaji, Estimation of parameters in multi-mode heat transfer problems using Bayesian inference - Effect of noise and a priori, Int J Heat Mass Tran 51 (9-10) (2008) 2313–2334.
[40] M.A.S. Iglesias, Zaid, Marco Scavino, Raúl Tempone, Christopher Wood, Bayesian inferences of the thermal properties of a wall using temperature and heat flux measurements, Int J Heat Mass Tran 116 (2018) 417–431.
[41] R.R. Raj, G. Venugopal, M.R. Rajkumar, Bayesian inference for parameter estimation in transient heat transfer experiments, J Heat Trans-T ASME 137 (12) (2015).
[42] J.B. Wang, N. Zabaras, A Bayesian inference approach to the inverse heat conduction problem, Int J Heat Mass Tran 47 (17-18) (2004) 3927–3941.
[43] W.K. Hastings, Monte Carlo sampling methods using Markov chains and their applications, Biometrika 57 (1) (1970) 97–109.
[44] N. Metropolis, A.W. Rosenbluth, M.N. Rosenbluth, A.H. Teller, E. Teller, Equation of state calculations by fast computing machines, 21(6) (1953) 1087-1092.
[45] R.C. Team.R: A language and environment for statistical computing, R Foundation for Statistical Computing, Vienna, Austria, 2013.
[46] W. Choi, H. Kikumoto, R. Choudhary, R. Ooka, Bayesian inference for thermal response test parameter estimation and uncertainty assessment, Appl. Energy 209 (2018) 306–321.
[47] K. Yoo, J. Shim, P. Dutta, Effect of Joule heating on isoelectric focusing of proteins in a microchannel, Biomicrofluidics 8 (6) (2014).
[48] J. Shim, P. Dutta, C.F. Ivory, Finite volume methods for isotachophoretic separation in microchannels, Numerical Heat Transfer, Part A: Applications 52 (5) (2007) 441–461.
[49] I.B. Sprague, P. Dutta, Modeling of diffuse charge effects in a microfluidic based laminar flow fuel cell, Numerical Heat Transfer, Part A: Applications 59 (1) (2011) 1–27.